

Molecular Structure, Vinyl Rotation Barrier, and Vibrational Dynamics of 2,6-Dichlorostyrene. A Theoretical and Experimental Research

Antonio A. Ceacero-Vega,[†] Tomás Peña Ruiz,[†] Manuel Fernández Gómez,^{*,†} José M. Granadino Roldán,[†] Amparo Navarro,[†] M. Paz Fernández-Liencres,[†] and Upali A. Jayasooriya[‡]

Department of Physical and Analytical Chemistry, University of Jaén, Campus Las Lagunillas E23071 Jaén, Spain, and School of Chemical Sciences and Pharmacy, University of East Anglia, Norwich NR4 7TJ, United Kingdom

Received: March 6, 2007; In Final Form: April 27, 2007

The molecular structure of 2,6-dichlorostyrene has been analyzed at MP2 and DFT levels using different basis sets concluding in a nonplanar geometry. The influence of either the level of theory or the nature of the substituent has been assessed. The vinyl–phenyl torsion barrier has also been investigated as a function of level of theory. The ultimate factors responsible for the torsion barrier have been studied using two different partitioning schemes, i.e., the total electronic potential energy and the natural bond orbital, NBO. A topological analysis of the electron density within the atom-in-molecule, AIM, theory predicts soft intramolecular chlorine (ring)–hydrogen (vinyl) contacts when the system becomes planar. A first complete vibrational study has been performed using theoretical data and experimental vibrational frequencies from IR, Raman and, for the first time, inelastic neutron scattering, INS, spectra. The new assignment proposed is based on a scaled quantum mechanical, SQM, force field and the wavenumber linear scaling, WLS, approach.

Introduction

The steadily increasing use of semiconductor materials has made for polymers with high refractive index to grow in applications ranging from light-emitting diode (LEDs) to planar light wave circuits. Polymers with high refractive index find a great deal of applications in optics and photonics due to their ability to reduce reflection losses at interfaces and, hence, increase light output (see, for instance, <http://www.brewer-science.com>). Besides the uses derived from their mechanical properties, this type of polymer allows the improved performance of many opto-photonics devices and applications in the construction of more efficient beam splitters since they allow for diminishing the optical thickness of diffraction gratings.

Poly(2,6-dichlorostyrene), $n_D = 1.6248$, is a homopolymer which can be considered to belong to this group. Furthermore, it is interesting as a candidate to be one of the so-called telechelic polymers, useful to form thermoplastics and thermoplastic elastomers.¹ Showing a very good flame resistance, their optical and chemical resistance properties make them ideally suited for use as optically clear film gaskets which are thermally and oxidatively stable.

A step-by-step knowledge of structure–property relationships from molecular structure to macroscopic properties is necessary to optimize synthetic polymers. Therefore an improved understanding of the monomer structure is a very important contribution to this goal.

In addition, 2,6-dichlorostyrene applications range from ophthalmic implants² to the synthesis of nonlinear optical polymers³ and as an intermediate in many copolymerization processes.^{4,5}

Its occurrence in workplace air has also been the target of different studies (see, for instance, ref 6) due to its doubtful effects on human health.

Despite its interest, studies concerning molecular structure and vibrational spectra of 2,6-dichlorostyrene are scarce, incomplete and controversial. This paper is aimed at obtaining a deeper insight into these matters. Thus, different theoretical calculations, ab initio MP2 and DFT, have been performed within the isolated molecule approximation with an assortment of basis set and/or functionals. One of the most important aspects in halo-styrene derivatives concerns the planarity of the phenyl–vinyl system as well as the nature and magnitude of the torsional barrier of the vinyl moiety. This is important to assess the flexibility of the polymer chains, a basis of many structure–property relationships, for which torsional degrees of freedom are the key to understand the conformational changes along the polymer backbone.⁷

Molecular structure and conformation of 2,6-dichlorostyrene have been studied previously by different researchers. To our knowledge, the first research on this subject goes back to Scott and Scheraga.⁸ The authors extended a method suited for ethane like molecules based on exchange interactions of the electrons in bonds adjacent to the bond about which internal rotation occurs and van der Waals interactions to obtain a vinyl-ring dihedral angle of about 20–26°.

Later, Barfield et al.⁹ using the ¹H NMR long-range coupling constants between ring and vinyl protons of a set of ring-substituted styrenes and using semiempirical VB and OM/INDO methods for styrene estimated an average vinyl-ring dihedral angle between 30–50°.

Rendell and Burnell¹⁰ and Rendell et al.¹¹ also concluded that the system is not planar (vinyl-ring dihedral angle equals 45.4° ± 1.0°) by using NMR technique.

* Corresponding author. E-mail: mfg@ujaen.es.

[†] University of Jaén.

[‡] University of East Anglia.

Trovato et al.¹² on the basis of the changes observed in the intensity of electronic absorption spectra due to the occurrence of internal rotation in conjugated systems with steric hindrance and using semiempirical calculations concluded that 2,6-dichlorostyrene is a nonplanar molecule with a torsion angle around 50°.

As for the vibrational spectra, Ansari and Singh¹³ recorded for first time gas-phase IR spectra in the region 250–4000 cm⁻¹ for some dihalo-styrene derivatives. They stated that, although there is evidence for the nonplanarity of monosubstituted styrene derivatives due to the interaction between the vinyl moiety and the substituent groups, the feasibility of occurrence of this effect in the case of dichlorostyrenes is very small. They assumed the molecule to belong to the C_s point group in order to provide a qualitative analysis of the vibrational spectra.

Later, Nyquist¹⁴ recorded the IR spectra of different styrene derivatives in gas phase and in CCl₄ and CS₂ solution and established infrared group frequency correlations useful for spectra-structure identification. Nyquist concluded the steric factors drive the vinyl and phenyl groups in styrene to coplanarity for those cases where atoms or groups such as Cl and CH₃ are not substituted in the 2,6-positions.

No data, theoretical or experimental, concerning gas-phase molecular structure exist in the literature. In this work we have performed geometry optimizations at different levels of theory, MP2 and DFT, with different basis sets in order to study not only the planarity of the molecule free of any intermolecular interaction but also to get an estimate of the performance of these theoretical methods in the estimation of the torsional barrier of this system. The influence of the number, nature and positions of the ring substituents has been assessed by comparing with other halostyrene derivatives already studied^{15–18} although it can be anticipated that in the current case, the increased hindrance due to the occurrence of chlorine atoms in positions α – α' is expected to have a significant effect on both magnitude and shape of the torsion barrier.

The nature and magnitude of the intramolecular forces contributing to the ultimately adopted molecular geometry and the torsion barrier have been investigated both through the partitioning of the total potential energy and natural bond orbitals, NBO, theory.¹⁹ The existence of intramolecular non-bonding contacts has also been investigated by means of an electron density study within the Atom-in-Molecule (AIM) framework²⁰ using the criteria given by Koch-Popelier.^{21,53}

The vibrational spectrum has been analyzed using data from IR, Raman and, for the first time, INS spectra. The later is especially well suited for low-frequency vibrations where the torsional vinyl-ring movements have their largest contributions. The proposed assignments were assessed by the so-called wavenumber linear scaling, WLS^{22–23} and scaled quantum mechanical force field SQM methodologies.²⁴

Experimental

The experimental data used for the vibrational analysis come from the IR, Raman and inelastic neutron scattering (INS) spectra. Liquid-phase IR spectra were recorded for the neat liquid at room temperature and at 1 cm⁻¹ resolution using a FTIR Bruker Vector 22 spectrophotometer with CsI optics and a DTGS detector. Raman spectra for the neat liquid were recorded at a resolution of 2 cm⁻¹ using a FTRaman Bruker RF100/S spectrometer equipped with a Nd:YAG emitting at 1064 nm with a power of 500 mW and a liquid N₂ cooled Ge detector. The INS spectrum was obtained using the time-of-flight crystal analyzer (TFXA) spectrometer at the ISIS pulsed

neutron facility, Rutherford Appleton lab., Chilton, U.K., which has an energy resolution <2%. The counting time for the sample was approximately 24 h. The sample was in an Al sample cell and kept at $T < 20$ K. Low temperature used in the latter spectroscopy is to reduce the Debye–Waller factor or to sharpen the fundamental modes by diminishing the intensity of the phonon wings.

Computational Details. Geometry Calculations. Gaussian'03²⁵ suite of programs running on a ia64HP sever rx 2600 was used to perform all the calculations. After a first modeling with GaussView 3.07,²⁶ ab initio MP2 and DFT calculations were performed using standard gradient techniques, default convergence criteria and frozen core approximation. The basis sets used were 6-31G*, 6-311G**, and 6-311++G**²⁷ and, in the case of DFT calculations, cc-pVTZ.²⁸ Becke's hybrid exchange B3²⁹ was used as exchange functional and Lee–Yang–Parr nonlocal functional LYP^{30,31} and Perdew and Wang, PW91, gradient-corrected functional,³² were used as correlation functionals. Also, the mPW1PW91 model was used as a modified Perdew–Wang exchange functional and Perdew–Wang 91 correlation which enlarges its field of application.³³

A set of full relaxed geometry optimizations was carried out in order to gain an insight on the performance of the level of theory and basis sets in the prediction of the molecular structure and conformation of 2,6-dichlorostyrene. Stationary points were assessed through energy analytical second derivatives. Zero-point energy corrections have been neglected.

Natural Bond Orbitals NBO v.3.1,³⁴ as implemented in Gaussian'03 and atom-in-molecule AIM2000³⁵ packages, were used to simulate the charge-transfer processes and intramolecular contacts which eventually explain the ultimately adopted molecular conformation in 2,6-dichlorostyrene.

Vibrational Analysis. The force constants matrix originated from Gaussian03 in terms of Cartesian coordinates was transformed into a system of natural coordinates. In order to determine the best harmonic force field, the quadratic force constants matrix was scaled according to Pulay's SQM method by using the ASYM40³⁶ program. The inverse vibrational frequencies have been used as weights; zero weights were given to missing and uncertain frequencies. No empirical corrections of the theoretical geometry were used.

Results and Discussion

Molecular Structure and Conformational Analysis of 2,6-Dichlorostyrene Monomer. In Figure 1 it can be seen the atomic arrangement and numbering of 2,6-dichlorostyrene. The optimized structure obtained at MP2 and DFT levels with different basis sets and functionals along with the experimental one¹⁰ can be seen in Table 1S (see Supporting Information). The influence of the halide disubstitution on some selected molecular parameters has been assessed by comparison with those for styrene and some monochloroderivatives, calculated at the same levels of theory (Table 1). Thus, comparing to styrene, chlorine 2,6-substitution yields an enlargement, (sharpened at DFT/B3LYP level), for C₁–C₂, C₁–C₃, and C₁–C₈ bond lengths whereas a very small effect for monosubstituted derivatives is observed. Besides, a shortening of C₃–C₄, C₅–C₆, and C₆–C₇ bond lengths is observed while very small effect or no regular pattern exists for mono-haloderivatives. These results, along with the slight narrowing of C₁–C₃–C₄ bond angle, point out that chlorine 2,6-ring disubstitution tends to diminish the conjugation effects.

The sensitivity of the different molecular structure features, i.e., bond lengths and angles, on the method and basis sets can

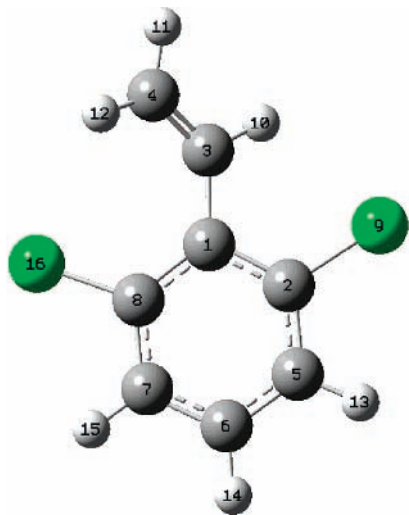


Figure 1. Spatial arrangement and numbering for 2,6-dichlorostyrene.

also be extracted from Table 1S. Here, we will only highlight the most significant ones.

Good indicators of the existence of π -conjugation in 2,6-dichlorostyrene are the vinyl C–C and the vinyl–phenyl C–C bond lengths. Theoretical values for C₁–C₃ bond length are intermediate between the experimental values for a typical C–C ethanelike single bond, 1.531 Å and a ethene like C=C double bond, 1.339 Å and somewhat longer than an aromatic benzene like C=C bond, 1.397 Å.²⁷ The inclusion of both polarization and diffuse functions on hydrogen atoms renders a slight but steady enlargement for this bond at MP2 level while the opposite is obtained with B3PW91 and mPW1PW91 functionals and shows no variation at B3LYP level. The results obtained with Dunning's correlation consistent basis set, cc-pVTZ, are remarkably shorter than those obtained with Pople's Gaussian ones for all cases. This vinyl-ring link compares well with the experimental value, 1.476 Å¹⁰, for which the maxima differences turn out to be 0.004 Å for mPW1PW91/6-311G** and 6-311++G** and 0.008 Å for mPW1PW91/cc-pVTZ. Since those experimental data¹⁰ were for a condensed phase and our theoretical calculations concern the isolated molecule, the closeness between both sets of geometrical parameters indicates a weakness of short-range anisotropic interactions among solvent and solute molecules.

The vinyl C–C bond, C₃–C₄, shows a similar, but more sensitive, dependence on the nature of the basis set. Thus, the maximum difference with respect to the experimental value, 1.339 Å,¹⁰ using Gaussian basis sets amounts to 0.004 Å for MP2/6-311++G**, whereas it is 0.008 Å for B3LYP and B3PW91 both with 6-311G** basis set and 0.011 Å for mPW1PW91/6-311G**. As for cc-pVTZ basis set, a shortening of 0.013 Å (mPW1PW91/cc-pVTZ) is observed.

As for the C–Cl bonds, the values obtained at DFT level show very small sensitivity on the Gaussian basis sets the maximum standard deviation being obtained for B3PW91, $\sigma_{n-1} = 8.94 \times 10^{-4}$ Å. This dependence is somewhat larger at MP2 level, $\sigma_{n-1} = 2.74 \times 10^{-3}$ Å. As before, cc-pVTZ values mean a shortening respect to Gaussian values irrespective of the functional used although it diminishes monotonically from B3LYP to mPW1PW91. In comparison to the experimental value 1.727 Å, all the theoretical results turn out to be longer, MP2/6-311G** and mPW1PW91/cc-pVTZ showing the lowest relative errors, i.e., 0.521% and 0.591%, respectively.

The theoretical values obtained with Gaussian basis sets for the vinyl–phenyl dihedral angle C₂–C₁–C₃–C₄, named θ

hereafter, show the nonplanarity of the system to range from 43.63° (B3LYP/6-31G*) to 55.84° (MP2/6-311++G**). DFT values compare well with the experimental value of 45.4°¹⁰ especially for mPW1PW91/6-31G* and are much closer to the experimental value than those obtained at MP2 level (maximum absolute error ca. 10° at MP2/6-311++G**). Also, for Dunning's basis set a small approximation toward the vinyl-ring coplanarity is observed irrespective the hybrid functional, this trend being slightly more noticeable at B3LYP level.

The sensitivity of θ on the basis set is greater than that for any other molecular parameter. Thus, the standard deviations, σ_{n-1} , for MP2 and DFT set of values, amount to 1.18° and 1.09° (B3LYP), respectively. Although MP2 values exhibit a monotonic trend as the basis set size increases, this is not the case for DFT calculations despite a similar pattern being observed for the three hybrid functionals used.

As for the bond angle C₂–C₁–C₃, cc-pVTZ values imply a very slight narrowing in comparison to Gaussian ones. All the theoretical values are close to the experimental value of 120.6°¹⁰ (maximum absolute error 1.06° for mPW1PW91/cc-pVTZ). This parameter shows a very small sensitivity on the basis set. Thus, MP2 values range within an interval of 0.1° while DFT values vary in a range of ca. 0.2° regardless of the hybrid functional used.

The Torsional Potential of 2,6-Dichlorostyrene. The planarity of the styrene derivatives will depend on a balance between two competing effects, π conjugation and steric effects involving the benzene ring and the vinyl moiety. The former preferring planarity, while the latter opposing planarity in order to avoid steric crowding. As the variation of C₁–C₃ and C₃–C₄ bond lengths as a function of the vinyl torsion angle seems to indicate, conjugation diminishes rather slowly as a function of the degree of nonplanarity,³⁸ so the departure of planarity of 2,6-dichlorostyrene lowers the steric strain at a nontotal loss of conjugation.

In this paper we analyze the torsional potential function of 2,6-dichlorostyrene in order to get an insight into the effects which govern the nature of the barrier, position of the minima and the influence of the level of theory and basis set on the relative energy barrier, and the relative stability of the different rotamers. All calculations have been made in a "relaxed" way, i.e., keeping fixed only the dihedral θ , and allowing all the other parameters to relax. The total energy surfaces (TESSs) have been constructed in steps of 5° or 10° using default convergence criteria as implemented in Gaussian'03. The energy profiles have been fitted to a sixth-order Fourier expansion

$$V(\theta) = V_0 + \sum_{i=1}^6 \frac{1}{2} V_{iN} (1 - \cos iN\theta) \quad (1)$$

where N , the symmetry number, turns out to be equal to 1. No contribution to torsional energies from zero-point energy ZPE, typically of 0.2 kcal/mol for conjugated systems,³⁹ has been taken into account. Theoretical values for potential parameters V_{iN} that best fit equation 1 (correlation coefficient $r^2 > 0.9999$) for 2,6-dichlorostyrene can be seen in Table 2. To the best of our knowledge, no experimental values for such potential parameters are known to be compared with the theoretical ones. A discussion about the physical meaning of such a set of coefficients is given in a next section.

Figure 2a–d shows torsional functions for each basis set at different levels of theory according to the trend 6-31G*/6-311G**/6-311++G**/cc-pVTZ. As can be seen, two stable conformers can be found in the interval $0 \leq \theta \leq 180^\circ$ at

TABLE 1: Theoretical Structure Parameters for 2,6-Dichlorostyrene as Compared with Others Styrene Derivatives

		C ₁ -C ₂	C ₁ -C ₃	C ₃ -C ₄	C ₂ -C ₅	C ₅ -C ₆	C ₆ -C ₇	C ₇ -C ₈	C ₈ -C ₁	C ₁ -C ₃ -C ₄
MP2/6-31G*	styrene ^a	1.405	1.472	1.343	1.394	1.397	1.396	1.395	1.404	125.3
	<i>cis-m</i> -chlorostyrene ^b	1.403	1.472	1.343	1.392	1.400	1.395	1.394	1.404	125.2
	<i>trans-m</i> -chlorostyrene ^b	1.403	1.472	1.343	1.393	1.394	1.396	1.394	1.404	125.2
	<i>p</i> -chlorostyrene ^c	1.404	1.471	1.343	1.393	1.396	1.395	1.395	1.404	125.4
	2,6-dichlorostyrene	1.408	1.476	1.340	1.393	1.393	1.393	1.396	1.408	124.1
B3LYP/6-31G*	styrene ^a	1.407	1.472	1.339	1.391	1.399	1.395	1.395	1.405	127.7
	<i>cis-m</i> -chlorostyrene ^b	1.407	1.473	1.338	1.389	1.396	1.394	1.394	1.405	127.6
	<i>trans-m</i> -chlorostyrene ^b	1.405	1.473	1.339	1.392	1.392	1.398	1.391	1.407	127.4
	<i>p</i> -chlorostyrene ^c	1.407	1.471	1.339	1.390	1.396	1.393	1.394	1.405	127.6
	2,6-dichlorostyrene	1.413	1.478	1.336	1.392	1.392	1.392	1.395	1.412	126.7

^a Ref 37. ^b Ref 16. ^c Ref 18.

TABLE 2: Parameters V(iN) for 2,6-Dichlorostyrene Fitting the Torsional Energy Function

	B3LYP			B3PW91				mPW1PW91				MP2
	6-31G*	6-311++G**	cc-pVTZ	6-31G*	6-311G**	6-311++G**	cc-pVTZ	6-31G*	6-311G**	6-311++G**	cc-pVTZ	6-31G*
V ₀	1.1295	1.1804	1.0565	1.4406	1.4348	1.2990	1.0863	1.5027	1.4637	1.3377	1.1223	3.0027
V ₁	-0.0040	-0.0273	-0.0147	-0.0343	-0.0380	-0.0303	-0.0194	-0.0338	-0.0379	-0.0315	-0.0185	-0.0996
V ₂	0.0118	-0.1329	0.1354	-0.3015	-0.5238	-0.3370	0.0647	-0.3343	-0.5127	-0.3399	0.1213	-2.2113
V ₃	-0.0021	-0.0047	-0.0475	-0.0487	-0.0355	-0.0384	-0.0443	-0.0482	-0.0347	-0.0397	-0.0485	-0.0340
V ₄	-1.1135	-1.1173	-1.1221	-1.2700	-1.1543	-1.1306	-1.1288	-1.3180	-1.1907	-1.1652	-1.1805	-1.6716
V ₅	0.0016	0.0481	0.0446	0.0564	0.0512	0.0512	0.0475	0.0558	0.0505	0.0503	0.0460	0.0894
V ₆	-0.0104	0.0049	-0.0910	-0.0314	-0.0062	0.0058	-0.0120	-0.0327	-0.0055	0.0078	-0.0076	-0.1952

45–50° and 130–140° for DFT and at 55° and 125° for MP2. Total energy wells are quasi-symmetrically located around the central hump at 90°. Relative energies for conformations at 0° and 180° are nearly identical regardless of the functional and basis set (maximum relative difference found 2.26% at B3PW91 and mPW1PW91 with 6-311++G**). Also, relative energy

values for planar conformations show a steady decreasing trend as the basis set size increases for B3PW91 and mPW1PW91. The central rotamer barrier height also shows a behavior strongly dependent on the level of theory and basis set. Hence, for Dunning's basis the barrier-height is the largest. As for MP2 results, they are at odds with DFT values with respect to the

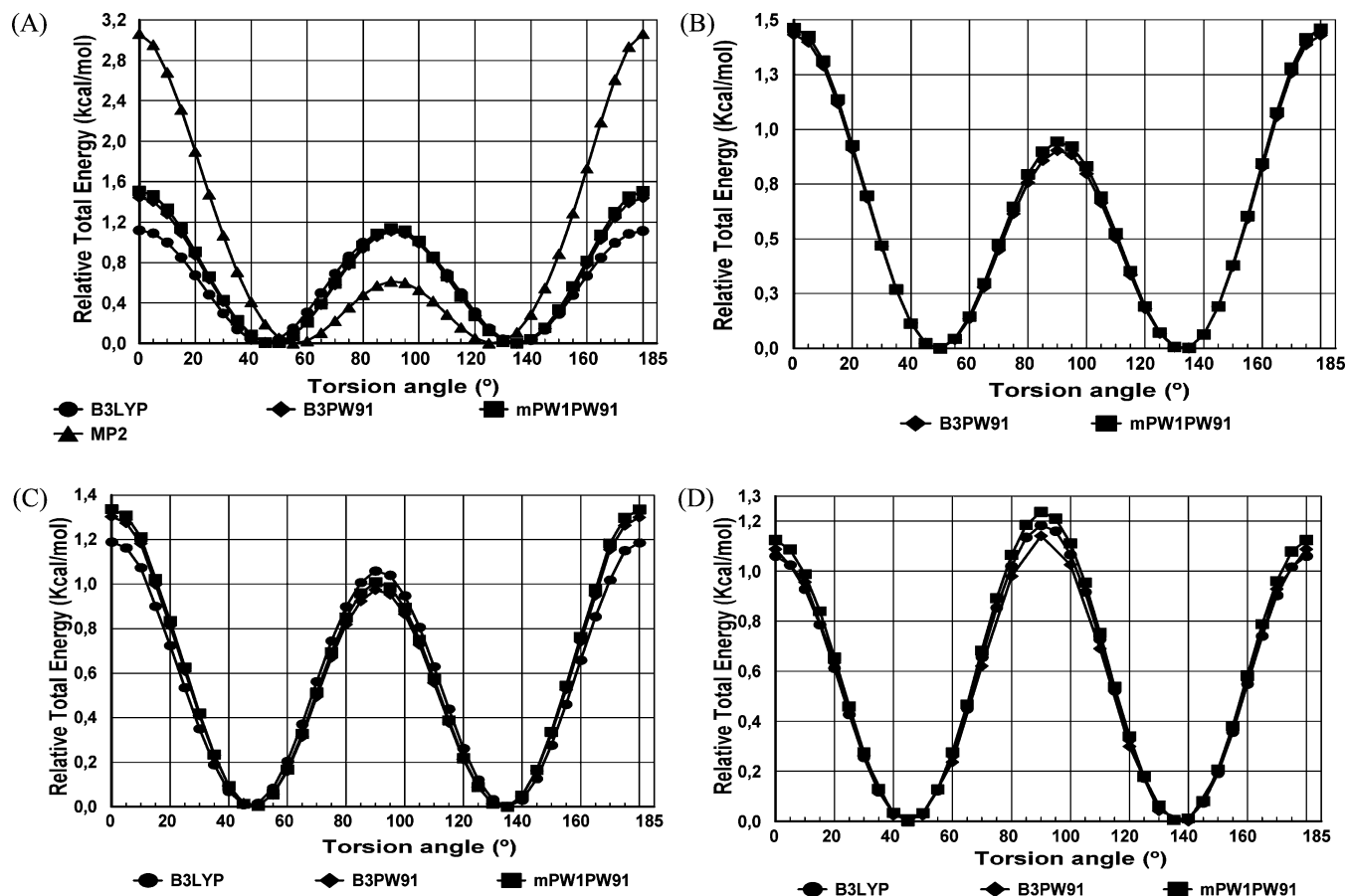


Figure 2. (a) 6-31G* total energy surface for the vinyl–phenyl torsion for 2,6-dichlorostyrene at different levels of theory. (b) 6-311G** total energy surface for the vinyl–phenyl torsion for 2,6-dichlorostyrene at different levels of theory. (c) 6-311++G** total energy surface for the vinyl–phenyl torsion for 2,6-dichlorostyrene at different levels of theory. (d) cc-pVTZ total energy surface for the vinyl–phenyl torsion for 2,6-dichlorostyrene at different levels of theory.

TABLE 3: (a) Evolution of C₃–C₄ Bond Length (Å) at Different Levels of Theory as the Torsion Angle θ Varies (in Deg); (b) Evolution of C₁–C₃ Bond Length (Å) at Different Levels of Theory as the Torsion Angle θ Varies (in Deg); (c) Evolution of C₃–C₄–C₁ Bond Angle (degrees) at Different Levels of Theory as the Torsion Angle θ Varies (in Deg)

θ	B3L YP			B3P W91				mP W1P W91				MP2
	6-31G*	6-311++G**	cc-pVTZ	6-31G*	6-311G**	6-311++G**	cc-pVTZ	6-31G*	6-311G**	6-311++G**	cc-pVTZ	6-31G*
	(a)											
0	1.3418	1.3396	1.3352	1.3408	1.3373	1.3385	1.3344	1.3384	1.3351	1.3364	1.3323	1.3469
10	1.3414	1.3391	1.3347	1.3403	1.3368	1.3380	1.3326	1.3380	1.3346	1.3359	1.3319	1.3464
20	1.3401	1.3377	1.3333	1.3391	1.3355	1.3366	1.3326	1.3367	1.3333	1.3346	1.3305	1.3451
30	1.3384	1.3357	1.3316	1.3375	1.3337	1.3347	1.3309	1.3352	1.3316	1.3327	1.3289	1.3435
40	1.3365	1.3336	1.3297	1.3359	1.3320	1.3327	1.3292	1.3336	1.3299	1.3307	1.3272	1.3419
50	1.3348	1.3317	1.3281	1.3345	1.3305	1.3309	1.3276	1.3322	1.3284	1.3289	1.3256	1.3406
60	1.3335	1.3302	1.3266	1.3333	1.3292	1.3295	1.3262	1.3310	1.3272	1.3276	1.3243	1.3396
70	1.3326	1.3291	1.3255	1.3323	1.3280	1.3285	1.3251	1.3300	1.3261	1.3266	1.3232	1.3391
80	1.3321	1.3285	1.3246	1.3316	1.3272	1.3279	1.3243	1.3293	1.3253	1.3260	1.3225	1.3389
90	1.3319	1.3283	1.3242	1.3313	1.3269	1.3277	1.3240	1.3290	1.3250	1.3258	1.3222	1.3387
	(b)											
0	1.4732	1.4717	1.4684	1.4691	1.4667	1.4669	1.464	1.4679	1.4657	1.4657	1.4630	1.4714
10	1.4733	1.4719	1.4687	1.4692	1.4671	1.4671	1.4642	1.4680	1.4657	1.4650	1.4629	1.4714
20	1.4745	1.4731	1.4695	1.4700	1.4680	1.4685	1.4651	1.4687	1.4666	1.4672	1.4639	1.4719
30	1.4761	1.4749	1.4709	1.4713	1.4694	1.4702	1.4665	1.4699	1.4680	1.4689	1.4652	1.4727
40	1.4782	1.4772	1.4728	1.4731	1.4714	1.4724	1.4684	1.4716	1.4699	1.4710	1.4670	1.4737
50	1.4808	1.4799	1.4753	1.4753	1.4738	1.4752	1.4709	1.4740	1.4722	1.4735	1.4694	1.4755
60	1.4837	1.4829	1.4781	1.4782	1.4766	1.4781	1.4738	1.4766	1.4748	1.4764	1.4722	1.4776
70	1.4866	1.4859	1.4813	1.4811	1.4796	1.4810	1.4770	1.4794	1.4777	1.4793	1.4752	1.4797
80	1.4888	1.4882	1.4841	1.4837	1.4822	1.4832	1.4798	1.4819	1.4804	1.4814	1.4780	1.4813
90	1.4896	1.4886	1.4853	1.485	1.4834	1.4838	1.481	1.4832	1.4815	1.4824	1.4792	1.4817
	(c)											
0	132.02	131.92	131.92	132.01	131.96	131.95	131.87	131.94	131.84	131.88	131.76	131.63
10	131.69	131.66	131.51	131.58	131.52	131.64	131.46	131.50	131.44	131.57	131.43	131.11
20	130.68	130.67	130.48	130.42	130.39	130.64	130.41	130.32	130.29	130.56	130.32	129.86
30	129.22	129.27	129.11	128.88	128.90	129.20	129.04	128.75	128.78	129.10	128.91	128.13
40	127.58	127.68	127.71	127.32	127.39	127.56	127.56	127.21	127.26	127.44	127.40	126.23
50	126.07	126.19	126.43	126.03	126.05	126.03	126.27	125.97	125.92	125.89	126.11	124.57
60	125.03	125.14	125.52	125.15	125.11	124.96	125.33	124.96	124.93	124.82	125.21	123.49
70	124.43	124.55	124.86	124.50	124.46	124.37	124.72	124.33	124.30	124.24	124.56	122.88
80	124.06	124.16	124.47	124.06	124.04	124.00	124.31	123.97	123.91	123.87	124.22	122.57
90	123.95	124.15	124.28	123.84	123.80	123.93	124.16	123.78	123.68	123.72	124.02	122.57

magnitude of the relative energy for the different conformations (Figure 2a). DFT barriers to torsion, defined as the energy difference between the well(s) and the central hump, range from 0.8685 kcal/mol (B3PW91/6-311++G**) to 1.2372 kcal/mol (mPW1PW91/cc-pVTZ), whereas for MP2/6-31G* a small barrier of 0.6127 kcal/mol is obtained.

A word of caution must be said, however. Since the torsion energy profiles have been evaluated from method-dependent optimized geometries, the results may be influenced by that dependence. However, a recent study on a selected set of π -conjugated molecules has shown that this influence on the relative energies, i.e., the torsional potentials, only amounts at most to 0.1 kcal/mol.⁴⁰

The influence of each level of theory at each one of the basis sets used can be seen in Figures 2a–d. They show the nearly energy equivalence between conformations at $\theta = 0^\circ$, where π -conjugation is maximum, and that at $\theta = 90^\circ$, for which π -conjugation should be minimized. It is noticeable that, when using Gaussian basis sets, the conformation at $\theta = 90^\circ$ is slightly more stable than the planar one while the opposite is observed for Dunning's basis set. MP2 results show that planar rotamer is remarkably less stable with an energy difference of ~ -2.311 kcal/mol. The relative energy gaps $E^{\text{MP2}} - E^{\text{DFT}}$ are, on average, -0.504 kcal/mol for $\theta = 90^\circ$ and 1.592 kcal/mol for $\theta = 0^\circ$. These results seem to indicate that additional stabilization for DFT π -conjugation is overstated, as appears in the literature [see for instance, ref 41].

In order to assess the relative magnitude of steric interactions and π -conjugation along the torsional potential, we have evaluated the evolution of such two parameters as the torsion

angle varies. The results can be seen in Tables 3a–c. C₃–C₄ bond lengths show a monotonic decrease from $\theta = 0^\circ$, where maximum conjugative effects are expected and minimum partial double bond character are expected, to $\theta = 90^\circ$ where the conjugative effects are minimized. This pattern is observed regardless of the level of theory and/or basis sets used. DFT values show an increasing relative variation as Gaussian basis set increases ranging from 0.70% (6-31G*) to 0.84% (6-311++G**). When using Dunning's basis set, a steady lowering is observed as the Hartree–Fock exchange percentage increases and the Perdew–Wang'91 nonlocal correlation⁴² is used, the relative variations ranging from 0.82% (B3LYP) to 0.76% (mPW1PW91). As for MP2 values, relative variation is 0.61%, significantly lower than DFT values.

The C₁–C₃ bond enlarges as θ increases, as expected. This effect is more significant for DFT values (average relative deviation $\sim 1.11\%$) than that for MP2 ones (0.70%). It is also observed that as the Gaussian basis set is augmented, the DFT lengthening average deviations also rise while cc-pVTZ deviations show no regular pattern as the functional varies.

The C₄–C₃–C₁ bond angle shows a sustained narrowing as θ increases, with the DFT results being slightly more sensitive when using Gaussian basis sets (6.12% average relative deviation) than those for Dunning's basis set (5.83%). MP2 values show the largest average deviation, i.e., 6.88%.

When compared to what is observed in styrene,⁴³ the C₃–C₄ bond length and C₄–C₃–C₁ bond angle show a steeper decreasing as θ increases what can be explained as a proof of the relevance of steric hindrances between nonbonded chlorine and vinyl-hydrogen.

Energy Decomposition of the Torsional Barrier for 2,6-Dichlorostyrene. Although only the total, kinetic, and potential energies have physical meaning, their expansion into different components, where possible, may help to understand the nature of interactions that shape the torsion barrier for 2,6-dichlorostyrene. Different schemes of decomposition may be performed.

In order to get a better comprehension on the nature of the DFT and MP2 torsion barriers, one approach consists of decomposing the energy into its components according to⁴⁴

$$\Delta E = \Delta E_k + \Delta V_{\text{tot}} = \Delta E_k + \Delta V_{\text{nn}} + \Delta V_{\text{ne}} + \Delta V_{\text{ee}} \quad (2)$$

where ΔE , ΔE_k , ΔV_{tot} , ΔV_{nn} , ΔV_{ne} , and ΔV_{ee} stand for the relative total, kinetic, total potential, nuclear–nuclear repulsion, electron–nuclear attraction and electron–electron repulsion energies, respectively, of each conformer with respect to the most stable one found at each level of theory according to the total energy value, i.e., 135°, 140°, and 125°, for B3LYP/6-311++G**, B3LYP/cc-pVTZ and MP2/6-31G*, respectively. Relative potential energy along with its components can be seen in Figure 3 for B3LYP/6-311++G**, B3LYP/cc-pVTZ and MP2/6-31G* (numerical values are reported in Table 2S). Note that in order to reproduce torsion energy curves (Figure 2a–d), kinetic energy must be added to the potential energy profiles (Figure 3).

Accordingly, three zones can be defined to explain the behavior of the energy as a function of the torsion angle. For $\theta \leq 45^\circ$, provided the attraction term V_{ne} is negative, B3LYP/6-311++G** (Figure 3A) predicts $\Delta V_{\text{ne}} > 0$ so that, as the molecule goes toward planarity, the attractive electron–nuclear energy diminishes attaining its minimum value when $\theta = 0^\circ$. As for ΔV_{nn} and ΔV_{ee} , they vary in a very similar fashion in magnitude and sign as well and they keep negative values regardless of the torsion angle in this interval. Since they are repulsive energies, that behavior means that they decrease in a monotonic trend up to their minimum value at 0° . Therefore, the top of total potential energy curve at $\theta = 0^\circ$ may be mainly ascribed to the dropping of attractive electron–nuclear forces rather than to an increase of repulsive nuclear–nuclear or electron–electron forces.

For $45^\circ < \theta < 135^\circ$, B3LYP/6-311++G** predicts $\Delta V_{\text{ne}} < 0$. The maximum negative values for ΔV_{ne} appear at $\theta = 60^\circ$ and 115° , whereas the minimum negative value is at $\theta \cong 90^\circ$. As for ΔV_{ee} , it is always positive getting its minimum value at $\theta = 90^\circ$ from two relative maxima at $\theta = 60^\circ$ and 115° approximately. The relative nuclear–nuclear repulsion energy, ΔV_{nn} , is positive except at $\theta \cong 90^\circ$ for which it is slightly negative (about 2 orders of magnitude smaller than ΔV_{ee}). Moreover, ΔV_{nn} diminishes from two relative maxima at $\theta \cong 60^\circ$ and 120° up to its minimum at $\theta \cong 90^\circ$. Therefore, the energy barrier at $\theta \cong 90^\circ$ cannot be explained claiming for an increase of the repulsive electron–electron and nuclear–nuclear energies but invoking a more important role in the diminution of the attractive electron–nuclear energy. The situation for $\theta \geq 135^\circ$ looks like that for $\theta \leq 45^\circ$.

For B3LYP/cc-pVTZ (Figure 3B) a very similar explanation can be given although new ranges for the torsion angle, i.e., $\theta \leq 40^\circ$, $40^\circ < \theta < 140^\circ$ and $\theta \geq 140^\circ$ as well as a slight shift in the angle at which the maxima and/or minima occur are noticed.

For MP2/6-31G* (Figure 3C) it is noticeable that ΔV_{ne} is positive while ΔV_{nn} and ΔV_{ee} are negative irrespective of the torsion angle. Also, it is noteworthy that the energy hump at 0° (and at 180°) can be explained claiming for a decrease of both nuclear–electron attraction energy and nuclear–nuclear and

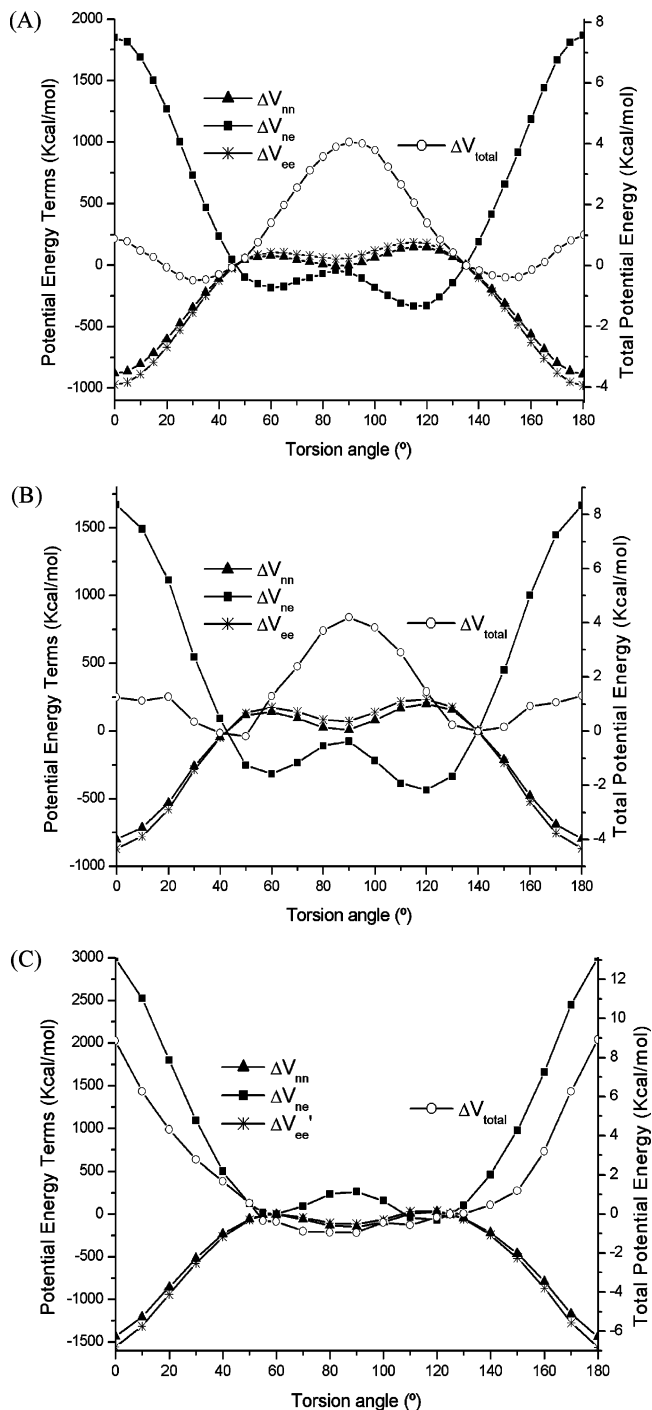


Figure 3. Torsion potential energy barrier decomposition for 2,6-dichlorostyrene (A) B3LYP/6-311++G**, (B) B3LYP/cc-pVTZ, and (C) MP2/6-31G*.

electron–electron repulsive energies as well. In the region defined by $55^\circ < \theta < 125^\circ$, repulsive energy terms prevail on the attractive one. Thus, the very low-energy barrier for the TES at $\theta = 90^\circ$ cannot be account for only from the total potential energy curve but it is necessary to take into account the kinetic energy term.

Furthermore, electron–electron repulsion energy V_{ee} within DFT theory can be split into three terms, i.e., Coulomb E_{Coul} , exchange E_{X} and correlation E_{C} energies. Table 4 shows their values as a function of the torsion angle for different levels of theory. For B3LYP with 6-311++G** and cc-pVTZ, it is noticeable the high value of the Coulomb energy ($\sim 107.6\% V_{\text{ee}}$) as compared to exchange ($\sim 7.4\% V_{\text{ee}}$ and $\sim 7.2\% V_{\text{ee}}$,

TABLE 4: Energy Components (au) of Electron–Electron Repulsion Energy as a Function of Basis Set and Vinyl–Phenyl Dihedral Angle, θ (Deg)

θ	B3LYP/6-311++G**			B3LYP/cc-pVTZ		
	E_{Coul}	E_{C}	E_{X}	E_{Coul}	E_{C}	E_{X}
0	1164.292	-4.122	-78.334	1166.307	-4.125	-78.330
40				1167.619	-4.124	-78.330
45	1165.796	-4.121	-78.333			
90	1165.929	-4.120	-78.331	1167.809	-4.123	-78.328
135	1165.838	-4.121	-78.333			
140				1167.697	-4.124	-78.330
180	1164.278	-4.122	-78.334	1166.309	-4.125	-78.330

respectively) and correlation ($\sim -0.40\%$ V_{ee} and $\sim -0.38\%$ V_{ee} , respectively) terms, regardless of the torsion angle. The absolute maxima values for E_{Coul} , E_{X} , and E_{C} appear at the top of the barrier $\theta = 90^\circ$, while the minima appear at $\theta = 0^\circ$ and 180° . As for the relative values ($V_{\text{ee}}(\theta) - V_{\text{ee}}(135^\circ)$) for B3LYP/6-311++G** and ($V_{\text{ee}}(\theta) - V_{\text{ee}}(140^\circ)$) for B3LYP/cc-pVTZ, the components show the same trend as the total electron–electron repulsion. Thus, we can conclude that the torsion barrier humps at 0° , 90° and 180° may be mainly ascribed to a decreasing of the so-called Coulomb term as far as ΔV_{ee} is concerned.

Another separation scheme in terms of NBO theory may be accomplished. Within the NBO analysis, the electronic wavefunction is interpreted as a set of occupied Lewis-type orbitals, paired with a set of formally unoccupied non-Lewis type orbitals. The electronic interactions within these orbitals, the deviations from the Lewis electronic structure, and the delocalization effects can be interpreted as charge transfer between the filled Lewis orbitals (donors) and the theoretically empty non-Lewis orbitals (acceptors).¹⁹

The magnitude of these delocalization effects, ΔE_{deloc} , can be determined directly by eliminating the charge transfer interactions using NOSTAR deletion. In addition, an analysis of the off-diagonal elements of the Fock matrix in the NBO basis taking account of all possible donor–acceptor interactions, and then calculating the strength of them all by second-order perturbation theory, $\Delta E^{(2)}$, provides further insight in the comprehension of ΔE_{deloc} and its structural consequences.

Thus, energy barrier can be written as a function of bond strength, hyperconjugation and steric repulsion according to⁴⁵

$$\Delta E_{\text{barrier}} = \Delta E_{\text{Lewis}} + \Delta E_{\text{deloc}} = \Delta E_{\text{struct}} + \Delta E_{\text{exc}} + \Delta E_{\text{deloc}} \quad (3)$$

The first term takes into account Coulomb and bond energy changes in the classical structure; the second term, known as Pauli exchange (or steric) repulsion, accounts for the non-Coulomb energy changes arising from Pauli exclusion principle according to which, pairs of electrons are not allowed to share the same spatial region. Finally, the third term describes the hyperconjugative stabilization.^{46,47} Second-order perturbation theory allows further details about the nature of these charge-transfer processes, ultimately responsible for the appearance of an extended molecular orbital that increases the stability of the system.

In Table 5 and Figure 4, contributions of Lewis and NOSTAR delocalization energies to the B3LYP/6-311++G** (cc-pVTZ) torsion barriers of 2,6-dichlorostyrene as a function of torsion angle can be seen. Accordingly, Lewis energy is the main barrier forming term for $\theta < 45^\circ$ (40°) and $\theta > 135^\circ$ (140°) while for 60° (55°) $\leq \theta \leq 120^\circ$ (140°) hyperconjugation term seems to be the responsible of the barrier. It is noteworthy that whereas Lewis' term plays a nearly null role in this range with 6-311++G** basis sets, this is not the case when cc-pVTZ basis set is used since Lewis' term is clearly anti-barrier forming.

TABLE 5: Contribution of Lewis and Delocalization Energies to the B3LYP/6-311++G and cc-pVTZ Torsion Barriers of 2,6-Dichlorostyrene as a Function of Vinyl–Phenyl Dihedral Angle, θ (Deg)**

θ	E_{rel} (kcal/mol)	$E_{\text{(Lewis)}}$ (au)	ΔE_{Lewis} (kcal/mol)	$E_{\text{(deloc)}}$ (au)	$\Delta E_{\text{(deloc)}}$ (kcal/mol)
B3LYP/6-311++G**					
0	1.063145	-1228.05867	7.153519	-0.906205	-6.09061
45	-0.000023	-1228.07002	0.026133	-0.896541	-0.02635
90	0.964723	-1228.06992	0.089962	-0.895105	0.87474
135	0.000000	-1228.07007	0.000000	-0.896499	0.00000
180	1.063523	-1228.05868	7.144754	-0.906190	-6.08119
B3LYP/cc-pVTZ					
0	1.045855	-1228.02800	6.077995	-0.984119	-5.03200
40	0.022094	-1228.03496	1.712108	-0.978793	-1.68988
90	1.171238	-1228.04082	-1.966864	-0.971099	3.13818
140	0.000000	-1228.03769	0.000000	-0.976100	0.00000
180	1.047376	-1228.02797	6.096011	-0.984146	-5.04895

Also, the hyperconjugation term is noticeably greater than that for 6-311++G** at a dihedral angle of 90° , thus showing a marked barrier forming character.

The main hyperconjugative interactions, calculated using second-order perturbation theory for the perpendicular, most stable nonplanar and planar conformations for B3LYP/6-311++G**, B3LYP/cc-pVTZ and MP2/6-31G* appear collected in Table 3S. As regards the interactions between chlorine lone pairs, LP, and the phenyl group the most significant contributions are due to LP Cl(9) $\rightarrow \pi^*$ (C_2-C_3) and LP Cl(16) $\rightarrow \pi^*$ (C_1-C_8). They all show little sensitivity to the torsion angle and they seem to favor slightly the perpendicular conformation. Concerning vinyl–phenyl interactions the most significant contributions come from $\pi_{\text{phenyl}} \rightarrow \pi^*_{\text{vinyl}}$ and $\pi_{\text{vinyl}} \rightarrow \pi^*_{\text{phenyl}}$ charge transfers. They all show a sharpen dependence on the torsion angle and they seem to favor the planar conformation. Finally, as to LP(Cl) $\rightarrow \sigma^*$ ($\text{C}-\text{H}$)_{vinyl} interactions, they only appear when the conformation becomes planar and thus it may justify the appearance of weak Cl \cdots (H–C)_{vinyl} contacts as AIM theory states (see next section). These conclusions can be drawn regardless of the level of theory and basis set used. Thus, after gathering the different components of the hyperconjugative interactions, we can think of the NOSTAR delocalization energy as mainly due to LP(Cl) $\rightarrow \sigma^*$ ($\text{C}-\text{H}$)_{vinyl} and phenyl–vinyl charge transfers.

Finally, a Fourier decomposition of the torsional energy may be accomplished. This analysis is not expected to provide any added value to the knowledge on the torsion barrier attained from the previous analysis except the searching for a physical meaning of the Fourier V_i coefficients. B3LYP/6-311++G**, B3LYP/cc-pVTZ, B3PW91/6-311++G**, and MP2/6-31G* levels has been selected as representative cases. According to the values for V_i reported in Table 2, the torsion energy is deconvoluted as shown in Figures 5a–d. As a result, 4-fold V_4 and 2-fold V_2 terms mostly govern the shape of these energy plots. It is noticeable that V_4 is neither method- nor basis-

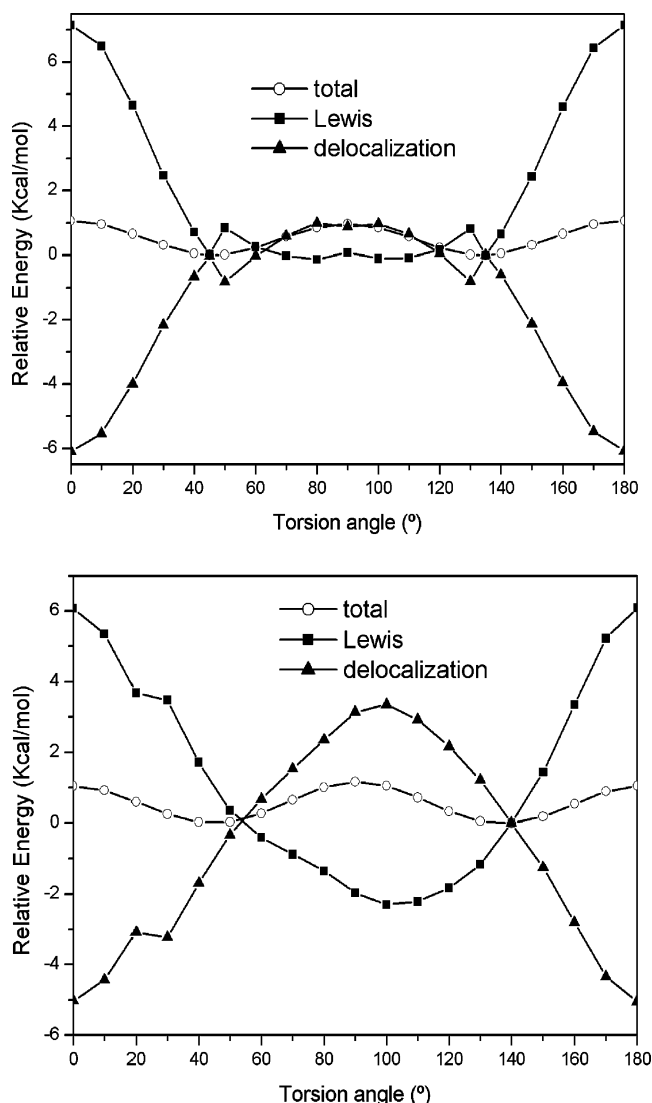


Figure 4. Lewis and NOSTAR delocalization energies contributions to the total relaxed torsion barrier energy of 2,6-dichlorostyrene: B3LYP/6-311++G** (up) and B3LYP/cc-pVTZ (down).

sensitive as regards the sign (negative) while V_2 shows a strong dependence either in magnitude and sign on the method and basis set. Accordingly, V_4 term turns out to be barrier forming for each level of theory used while V_2 term is barrier forming in the case of B3LYP/cc-pVTZ. It is also noteworthy that for MP2/6-31G*, V_2 gets a much larger value than that for V_4 and gives rise to a very low-energy barrier at $\theta = 90^\circ$. The Fourier analysis of torsional barriers in terms of hyperconjugative, conjugative, steric and/or electrostatic interactions is a useful tool for investigating the nature of the interactions within the molecular system. In general, the V_2 term is associated with the conjugative effects that have a periodicity of 180° whereas nonbonding interactions contribute to all the terms.^{48–51}

The negative V_2 favors the perpendicular rotamer ($\theta = 90^\circ$). Since conjugation is not favored in the perpendicular conformation, the contribution of V_2 to the torsion barrier represents other possible hyperconjugative interactions. They are collected in Table 3S and represent the lone pair donation from the chlorine atoms to the C–C bond in the benzene ring. These conclusions may straightforwardly be drawn for MP2/6-31G* while for B3LYP is not so clear since the very small value (negative for B3LYP/6-311++G** and positive for B3LYP/cc-pVTZ) for V_2 renders very small differences of the stabilization energies

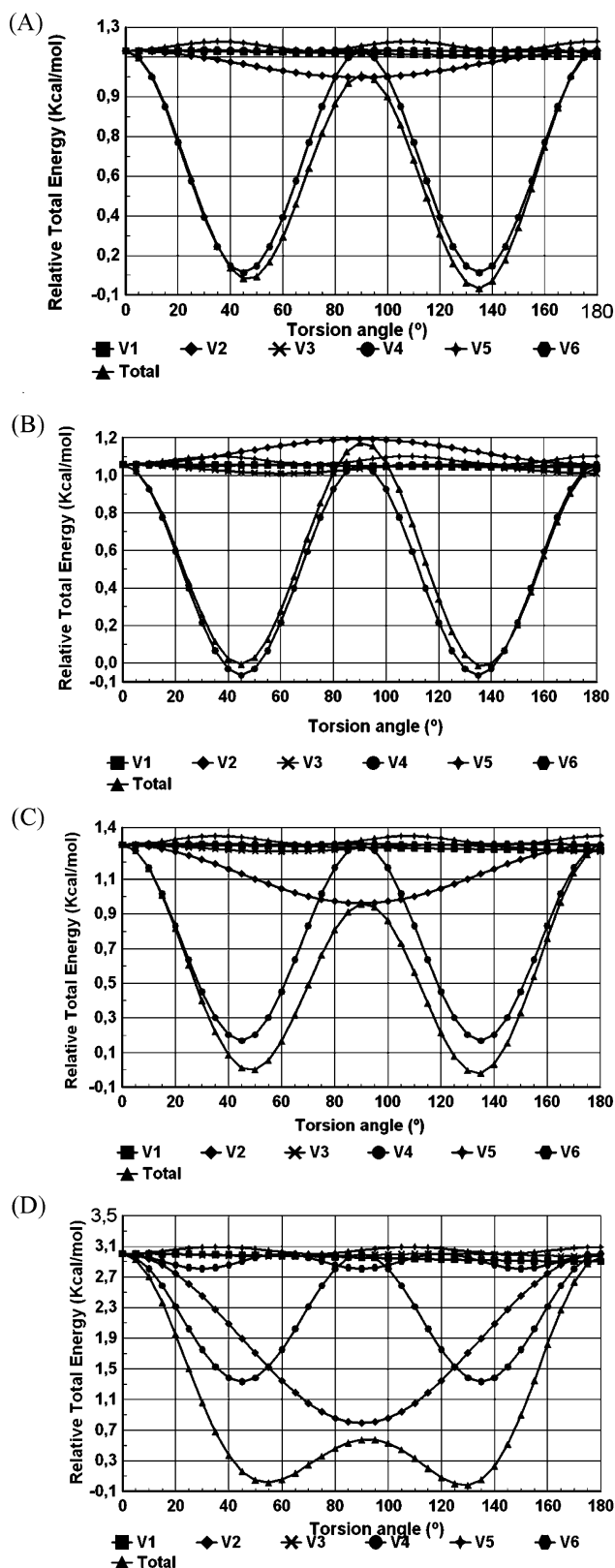


Figure 5. Total energy profile deconvolution for (A) B3LYP/6-311++G**, (B) B3LYP/cc-pVTZ, (C) B3PW91/6-311++G**, and (D) MP2/6-31G* for vinyl–phenyl torsion angle of 2,6-dichlorostyrene.

which prevent us from concluding not only about the structural preference due to hyperconjugative interactions but even about the ultimate energy-meaning of such a coefficient V_2 .

This theory level-dependent role of V_2 appears again into the total energy partitioning scheme. However, the relatively larger

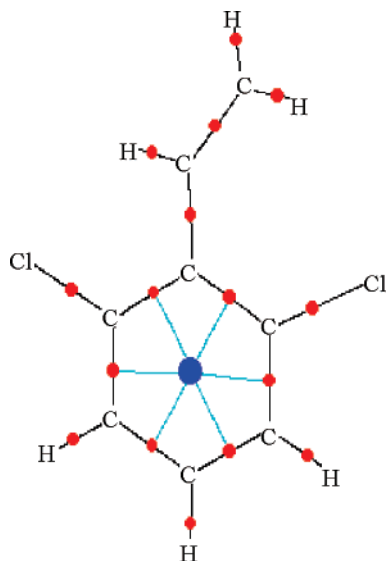


Figure 6. Bond critical points (red) and ring critical points (blue) for the twisted conformer of 2,6-dichlorostyrene.

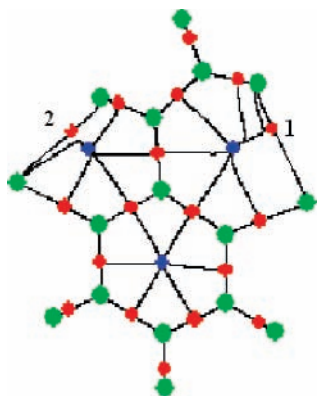


Figure 7. Bond (red) and ring (blue) critical points for planar 2,6-dichlorostyrene.

negative value V_4 term favors conformations with $\theta = 45^\circ$ and 135° , as expected. According to the total energy partitioning scheme, V_4 might be related to the diminution of nuclear-electron attraction while in terms of NBO theory, it might be mainly ascribed to Lewis energy term for $\theta < 45^\circ$ ($\sim 55^\circ$) and $\theta > 135^\circ$ (140°) for B3LYP/6-311++G**(cc-pVTZ), which according to equation 3 represents electrostatic contributions and/or steric repulsion.

Topological Analysis of the Electron Density. Apart from the delicate balance among the different contributions to the molecular energy, the nonplanar conformation of 2,6-dichlorostyrene may be due to the existence of intramolecular interactions like weak halogen-hydrogen-bonding that eventually can contribute to stabilize it. In order to get an insight into this matter we have made use of the “atom in molecule” approximation⁵² that through the Ehrenfest and Feynman theorems as well as the virial theorem, describes the forces acting in a molecule and the molecule’s energy related to them. As a result, Bader’s AIM theory relies on the localization of the so-called (3,−1) type bond critical points, BCP, of the distribution $\rho(r)$, i.e. those

satisfying $\nabla \rho(r) = 0$ and also of positive laplacian, $\nabla^2 \rho(r) > 0$, pointing in such a case that the charge density withdrawal toward each atom. In order to check the weak intramolecular interactions in 2,6-dichlorostyrene eight criteria proposed by Koch-Popelier²¹ and Popelier⁵³ are used. The reference non-bonded molecular structure adopted has been that optimized at B3LYP/6-311++G** (torsional angle approximately 45°) while the bonded molecular structure has been the planar structure (a saddle point) obtained at the same level.

In Figure 6 the critical points for the nonplanar conformation can be seen. Only bond critical points (red) for C–C, C–H and Cl–C bonds as well as a ring critical point (blue) can be noted but no critical point involving $\text{Cl}\cdots\text{H}_{\text{vinyl}}$ appears. Figure 7 shows bond (red) and ring (blue) critical points for planar 2,6-dichlorostyrene.

Numerical results (in au) for Popelier’s criteria for BCP’s 1 and 2 for planar 2,6-dichlorostyrene can be seen in Table 6. Accordingly, the electron density at the BCP’s falls in between the range given by Popelier’s criteria for such property, i.e., 0.002–0.035 au. Laplacian of the electron density at the BCP’s turns out to be 0.062 and 0.068 for BCP 1 and 2, respectively and they are well within the range established for that according Popelier’s criteria, i.e., 0.024–0.139 au. Ellipticity measures the extent to which charge is preferentially accumulated. It provides a criterion for structural stability in such a manner that the larger the ellipticity the weaker the bond. Thus, $\text{Cl}_{16}\cdots\text{H}_{12}$ bond (BCP no. 1, see Figure 7) turns out to be stronger than $\text{Cl}_9\cdots\text{H}_{10}$ bond (BCP no. 2). As for the mutual penetration of the hydrogen and acceptor atoms, it is considered as a necessary and sufficient condition to fully describe a hydrogen bond. It compares the nonbonded radii of the donor-hydrogen and the acceptor atoms with their corresponding bonding radii, taken as the distances from the nucleus to the BCP, i.e., Δr_d and Δr_a , respectively. Thus, if $\Delta r_d > \Delta r_a$ and $\Delta r_d + \Delta r_a > 0$, simultaneously, we can think of a genuine hydrogen-bond while if not, the interaction is van der Waals in nature.⁵⁴ For planar 2,6-dichlorostyrene, $\Delta r_d = 0.0738$ au and $\Delta r_a = 0.0542$ au (mutual penetration, 0.1280 au) for BCP 1, whereas for BCP 2, $\Delta r_d = 0.0581$ au and $\Delta r_a = 0.0350$ au (mutual penetration, 0.0931 au).

The increased net charge of hydrogen atoms, $q(\Omega)$, allows getting an insight of the H-bonding strength as a function of electron losses. In our case, both hydrogen atoms show small electron losses pointing toward the weakness of the hydrogen bonds. The energetic destabilisation of the hydrogen atom, $E(\Omega)$, means that the energy of the hydrogen atom will rise upon hydrogen-bonding formation. The results show that there exists indeed an increasing of the energy atom upon the formation of hydrogen bonding. The decreasing of dipolar polarization $M(\Omega)$ of the hydrogen atom also comes through the formation of an hydrogen-bond. In our case, this decreasing is noted for both H_{10} and H_{12} being more noticeable for BCP 1. Finally, volume $V(\Omega)$ of hydrogen atoms should diminish upon the formation of hydrogen bonding as it is the case for both BCPs 1 and 2 (see Table 6). Thus, we can conclude that for planar conformation there exist two soft critical points that seem to confirm the existence of two weak nonbonding halogen–hydrogen (vinyl) interactions but they are not strong enough to prevail over other nonattractive interactions that make the twisted conformation

TABLE 6: Popelier’s Criteria for Planar Configuration of 2,6-Dichlorostyrene

BCP	electron density	Laplacian	ellipticity	mutual penetration	$q(\Omega)$	$M(\Omega)$	$V(\Omega)$	$E(\Omega)$
1	0.016	0.062	0.068	0.1280	−0.030 3	−0.002 7	−6.718 9	0.0149
2	0.017	0.068	0.277	0.0931	−0.018 3	−0.001 4	−6.615 5	0.0077

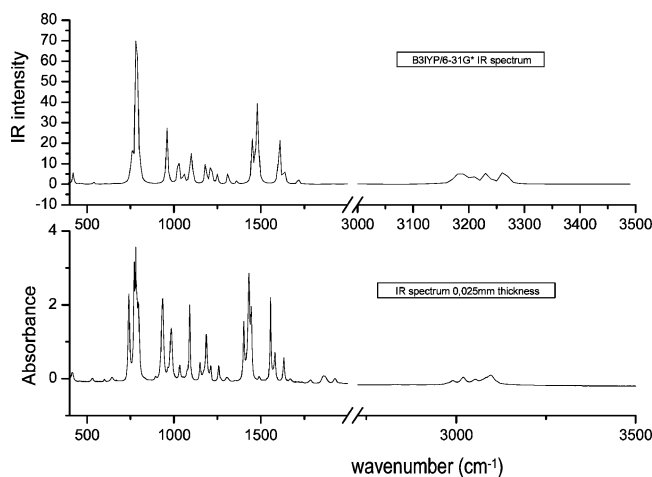


Figure 8. IR spectrum, simulated (up), and experimental (down) of 2,6-dichlorostyrene.

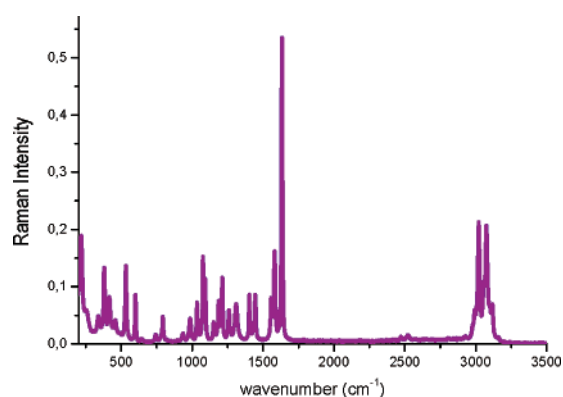


Figure 9. Raman spectrum of liquid 2,6-dichlorostyrene.

to be more stable. This conclusion is reinforced by NBO second-order perturbation treatment (see Table 3S) according to which $LP(Cl) \rightarrow \sigma^*(C-H)_{\text{vinyl}}$ charge transfer only appears when planar conformation is considered.

Vibrational Analysis of 2,6-Dichlorostyrene. In this report a new vibrational assignment is proposed on the basis of a theoretical force field using the Scaled Quantum Mechanical (SQM) approach^{24,55,56} as well as Yoshida's Wavenumber Linear Scaling (WLS) methods.^{22,23}

In Figure 8 (down) the experimental IR spectrum recorded with a sample of 0.025 mm thickness and after 50 scans can be seen. Also, Figure 8 (up) shows the simulated IR spectrum at DFT B3LYP/6-31G* that is used as a starting point to perform the subsequent vibrational analysis. Figure 9 shows the experimental Raman spectrum collected at 90° geometry and of 100 scans. Finally, Figure 10 shows the INS spectrum of 2,6-dichlorostyrene.

B3LYP/6-31G* theoretical vibrational frequencies in the harmonic approximation have been calculated at the stationary point by using the energy analytical second derivatives. Numerical results can be seen in Table 7.

Despite the good performance of B3LYP hybrid functional to predict vibrational frequencies, there exists a number of shortcomings that theoretical methods share when used to calculate the vibrational spectrum of a system, i.e., the effect of the incompleteness of the basis set, the incomplete treatment of the electron correlation and the presence of anharmonicity. A less computational demanding way to remove these disadvantages consists of applying a number of methods which scale theoretical quadratic force constants or theoretical vibrational

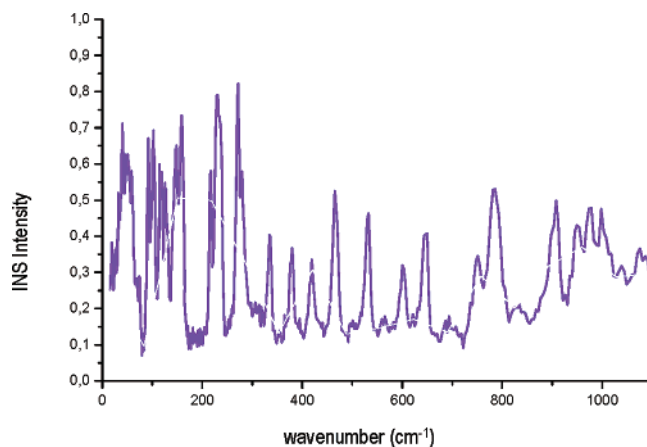


Figure 10. INS spectrum of solid 2,6-dichlorostyrene.

frequencies. It is implicitly assumed that these scaling factors correct for most of the errors the theoretical frequencies bear due to be harmonic.

Scaled Quantum Mechanical Force Field (SQM). Harmonic vibrational frequencies are calculated by diagonalizing the Hessian matrix, i.e., the second-order derivatives matrix of the electronic energy. Since the related quantities are the force constants, it is not surprising that the first attempt to correct the theoretical results by means of empirical scaling factors would act on the above-mentioned quantities. One of the most widely applied and accepted methods is the scaled quantum mechanical, SQM, method. This procedure^{24,55,56} is based on the transferability of the force constants and dipole moment derivatives among similar molecules. The procedure does not assume that the force constants are similar in related molecules, but makes the weaker assumption that the error in calculating a force field is similar for related types of vibrational motions in related molecules as calculated by identical computational procedure. Within the SQM technique, an initial set of theoretical force constants, F^{Theo} , is scaled by a diagonal matrix S , which contains the so-called scaling factors, according to the matrix relationship $F^{\text{Scal}} = S^{1/2} F^{\text{Theo}} S^{1/2}$ in such a manner that any diagonal force constants F_{ii} is scaled by the scale factor S_{ii} while an off-diagonal force constant F_{ij} appears scaled by $(S_{ii} S_{jj})^{1/2}$. The advantage of this method is its extreme simplicity and that it turns out to be theoretically justified as well.⁵⁷ In particular, scaling with several scale factors requires the transformation of the theoretical force field to a complete, nonredundant chemically reasonable local internal coordinate system, called natural internal coordinates, (see Table 8) which provides a strong chemical meaning for vibrations.^{55,56}

Figure 11 shows the natural internal coordinates for 2,6-dichlorostyrene, where τ_{55} and τ_{56} stand for torsion angles defined according to Hilderbrant.⁵⁸

The scaling procedure has been carried out in different steps. First a unique scale factor, 0.928 as recommended by Rauhut et al.⁵⁹ for B3LYP/6-31G* level was used regardless of the internal natural coordinate. Then, this unique factor was refined in order to fit the experimental frequencies. Afterward, a set of 14 independent scale factors associated with the natural internal coordinates was used; and finally this set was also refined in order to reproduce the experimental frequencies. The scaling and refinement have been performed by using ASYM40.³⁶ The values of initial and final scaling factors can be seen in Table 9.

In Table 4S we report the force constants both initial, as obtained from Gaussian 03, and those obtained after the scaling and refinement of the scale factors. In Table 10 experimental

TABLE 7: Observed, Calculated, and SQM Scaled Vibrational Frequencies (cm⁻¹) and Approximate Description of Vibrational Movements of 2,6-Dichlorostyrene^a

mode	observed					SQM		approximate description
	IR	Raman	INS	Ansari & Singh [13]	B3LYP/6-31G*	(A)	(B)	
1	3095m	3118			3264	3144	3130	(C _{vinyl} -H) st
2		3099			3233	3115	3101	(C _{ring} -H) st
3	3083sh	3076		3085	3229	3110	3097	(C _{ring} -H) st
4	3053vw	3058		3045	3206	3088	3075	(C _{ring} -H) st
5	3020w	3021		3012	3186	3069	3056	(C _{vinyl} -H) st
6	2991w	2993		2985	3175	3059	3046	(C _{vinyl} -H) st
7	1632m	1634		1628	1716	1652	1649	(CC) _{vinyl} st, (C _{ring} -H) rock
8	1581m	1582		1578	1636	1575	1582	(CC) _{ring} st, asym. ring def.
9	1556s	1557		1552	1607	1547	1554	(CC) _{ring} st, (C _{ring} -H) rock, asym. ring def.
10	1444m	1446	1443	1442	1488	1433	1440	(C _{vinyl} -H) bend., (CC) _{vinyl} st
11	1432vs	1434	1427	1430	1477	1423	1433	(C _{ring} -H)rock, (CC) _{vinyl} st.
12	1402m	1403	1409	1400	1452	1398	1404	(C _{ring} -H) rock, (C _{vinyl} -H) bending
13	1305vw	1310	1359	1350	1360	1310	1320	(C _{vinyl} -H) rock
14	1258m	1259	1260	1258	1312	1264	1264	(CC) _{ring} st
15	1212m	1214	1224	1210	1249	1203	1214	(CC) _{ring} st, (C _{ring} -H) rock, (C C) _{vinyl} st
16	1186s	1188	1188	1185	1214	1170	1178	(C _{ring} -H) rock, (CC) _{ring} st, (C C) _{vinyl} st
17	1150m	1152	1153	1148	1183	1139	1152	(C _{ring} -H) rock
18	1091s	1092	1087	1090	1110	1069	1085	(CC) _{ring} st, (C _{ring} -H) rock
19	1078sh	1077	1076		1097	1056	1076	(C _{vinyl} -H) st, (C-Cl) st, (CC) _{ring} st, (C _{vinyl} -H) rock
20	1033m	1035	1044	1032	1056	1017	1035	(C _{vinyl} -H) rock, trig. ring def.
21	984s	986	1018	983	1026	988	1001	(CC) _{vinyl} tors, (CC) _{vinyl} wag
22	966sh		950		973	937	965	(C _{ring} -H) wag, ring puck.
23	934s	935	936	932	960	924	948	(CC) _{vinyl} wag
24	895sh		908	892	904	871	896	(C _{ring} -H)wag
25	794sh	793	805		804	775	795	asym. ring def., (CC) _{vinyl} st, Trig. ring def.
26	781sh		786		789	760	785	ring puck., (C _{ring} -H) wag., (C _{ring} -Cl) wag.
27	775vs		781	775	783	754	777	asym. ring. def., (C-Cl) st., (C _{ring} -H) wag.
28	740s	742	751	740	757	729	743	ring puck., benzene wag., (C _{ring} -H)wag., (C _{ring} -Cl)wag
29	644vw		650		655	630	639	ring puck, vinyl wag., (CC) _{vinyl} tors
30	600vw	601	600		606	584	598	asym. ring def., ring puck, sym. vinyl def.
31	530w	532	546		539	519	532	asym. ring tor., (C _{ring} -Cl) wag
32			532	522	536	516	526	asym. ring tor., (C _{ring} -Cl) wag
33	458vw	459	465		467	449	462	asym. ring tor., ring wag., vinyl wag., asym. ring def.
34	418w	416	419		420	404	423	asym. ring def., (C _{ring} -H) rock
35	379w	380	379	415	380	366	392	(C _{ring} -Cl)rock, (C-Cl)st, asym. ring. def., sym. vinyl def.
36	336vw	339	335	345	336	324	340	(C _{ring} -Cl) rock, sym. vinyl def., asym. ring def.
37		254	261	330	261	251	262	vinyl rock, ring wag, vinyl torsion, (C _{ring} -Cl) wag
38		219	221		222	214	234	(C _{ring} -Cl) rock
39		214	213		213	205	212	vinyl rock, sym. vinyl def., ring wag, (C _{ring} -Cl)wag
40					202	195	196	asym. ring torsion
41					107	103	101	vinyl torsion, asym. ring tor, (C _{ring} -Cl) rock
42					69	66	66	vinyl torsion, sym. vinyl def., asym. ring tor.

^a vs, very strong; s, strong; m, medium; sh, shoulder; w, weak; vw, very weak. (A) Fitting using an unique scaling factor; (B) fitting using 14 scaling factors.

and calculated vibrational frequencies are reported along with the description of the normal modes according to the Potential Energy Distribution (PED) matrix. As expected, the fitting with the experimental frequencies improve a lot using the set of 14 refined scaling factors as shown by their rms deviations, 8 cm⁻¹ vs 22 cm⁻¹ when using one unique scale factor.

Wavenumber Linear Scaling (WLS). Another way of facing the above-mentioned problem is through the direct scaling of the theoretical vibrational frequencies. This method, proposed by Yoshida et al.,^{22,23} uses a linear relationship between the scaling factor, defined as the ratio between observed and calculated frequencies, and the calculated ones. For B3LYP/6-31G* level the linear equation is $(\nu_{\text{obs}}/\nu_{\text{cal}}) = 1.0 - 0.00002520 \nu_{\text{cal}}$, obtained after fitting of 17 fundamentals of indene in the fingerprint region. Table 10 reports the results of the wavenumber-linear scaling for 2,6-dichlorostyrene where ν_{obs} and ν_{cal} are the average observed and B3LYP/6-31G* frequencies respectively. The rms deviation amounts to 41 cm⁻¹.

It must be said that the scaling factors themselves carry uncertainty. This aspect has been discussed in detail by Irikura et al.⁶⁰ Accordingly, scaling factors are only accurate to two

significant digits. Thus, the last digit for scaling factors appears as uncertain in brackets, in Tables 9 and 10.

Assignment of the Vibrational Spectrum. The new assignment for the vibrational spectrum of 2,6-dichlorostyrene (Table 7) suggests significant changes with respect to that proposed by Ansari and Singh:¹³

(1) As for the region of C-H stretching, 2990 cm⁻¹ – 3110 cm⁻¹, the mode ν_1 , =CH₂ asymmetric stretching, is assigned to the Raman band at 3118 cm⁻¹ whereas Ansari and Singh assigned it to the band at 3085 cm⁻¹. Also, the normal mode ν_2 , C_{ring}-H stretching, is assigned in this paper to the band at 3099 cm⁻¹ (Raman) but remains unassigned by Ansari and Singh. The C_{ring}-H stretching mode ν_3 is linked to the shoulder at 3083 cm⁻¹ (IR) which corresponds to the recorded band at 3085 cm⁻¹ by Ansari and Singh. As regards, ν_4 , ν_5 and ν_6 , our assignment matches that by Ansari and Singh, although the bands are blue-shifted.

(2) As concerns the region, 700–1500 cm⁻¹ several changes are proposed. Thus, the mode ν_{11} , is described in this paper as a combination of C_{ring}-H rocking and (C-C)_{ring} stretching whereas it is a = CH₂ scissoring for Ansari and Singh. The

TABLE 8: Natural Internal Coordinates and Scale Factor Used for 2,6-Dichlorostyrene

coordinate number	description	definition
1–6	(CC) _{ring} St	R ₁ –R ₆
7	(C _{ring} –C _{vinyl})st	R ₇
8	(CC) _{vinyl} st	R ₈
9,13	(C–Cl) st	r ₉ , r ₁₃
10, 11, 12	C _{ring} –H st	r ₁₀ , r ₁₁ , r ₁₂
14, 15, 16	C _{vinyl} –H st	r ₁₄ , r ₁₅ , r ₁₆
17	trig. ring def.	($\alpha_{17} - \alpha_{18} + \alpha_{19} - \alpha_{20} + \alpha_{21} - \alpha_{22}$)/6
18	asym. ring def.	($2\alpha_{17} - \alpha_{18} + \alpha_{19} + 2\alpha_{20} - \alpha_{21} - \alpha_{22}$)/12
19	asym. ring def.	($\alpha_{18} - \alpha_{19} + \alpha_{21} - \alpha_{22}$)/2
20, 24	C _{ring} –Cl rock	($\alpha_{26,34} - \alpha_{27,35}$)/ $\sqrt{2}$
21, 22, 23	C _{ring} –H rock	($\alpha_{28,30,32} - \alpha_{29,31,33}$)/2
25	vinyl rock	($\delta_{24} - \delta_{25}$)/2
26, 27	C _{vinyl} –H rock	($\rho_{36,38} - \rho_{37,40}$)/2
28	sym. vinyl def.	($2\rho_{23} - \rho_{36} - \rho_{37}$)/6
29	C _{vinyl} –H bending	($2\rho_{39} - \rho_{38} - \rho_{40}$)/6
30, 34	Cb–Cl wag	γ_{41}, γ_{45}
31, 32, 33	Cb–H wag	$\gamma_{42}, \gamma_{43}, \gamma_{44}$
35	vinyl wag	γ_{46}
36	(CC) _{vinyl} wag	γ_{47}
37	ring wag.	γ_{48}
38	ring puck.	($\tau_{50} - \tau_{51} + \tau_{52} - \tau_{53} + \tau_{54} - \tau_{49}$)/6
39	asym. ring torsion	($\tau_{50} - \tau_{52} + \tau_{53} - \tau_{49}$)/2
40	asym. ring torsion	($2\tau_{51} - \tau_{50} - \tau_{52} - \tau_{53} + 2\tau_{54} - \tau_{49}$)/12
41	vinyl torsion	τ_{55}
42	(CC) _{vinyl} tors.	τ_{56}

latter authors describe ν_{12} as a C–C stretching vibration but it is a mixture of (C_{ring}–H) rocking and (C_{vinyl}–H) bending in our research. Ansari and Singh assign the mode ν_{13} to a band appearing at 1350 cm⁻¹ and describe it as a C–C stretching but in this work, we assign it to the band at 1310 cm⁻¹ (Raman) and it is a (C_{vinyl}–H) rocking vibration. According to the potential energy distribution matrix (PED) obtained in our research, ν_{14} is a (C–C)_{ring} stretching but it is a (C_{vinyl}–H) rocking in Ansari and Singh's paper. ν_{15} is a complex mode composed of (C–C)_{ring} stretching, (C_{vinyl}–H) rocking and (C–C)_{vinyl} stretching which is assigned to a (C–C)_{vinyl} stretching in reference (13). The band appearing at 1077 cm⁻¹ is assigned by us to the mode ν_{19} , a mixture of (C_{vinyl}–H) stretching and (C_{ring}–Cl) stretching, but remains unassigned by Ansari and Singh. The latter authors described the mode ν_{21} as a (C_{vinyl}–H) bending but our PED suggests a mixture of (C–C)_{vinyl} torsion and (C–C)_{vinyl} wagging. ν_{23} is described in this paper as a (C–C)_{vinyl} wagging but Ansari and Singh consider it as (C_{vinyl}–H) bending. The modes ν_{27} and ν_{28} are assigned in reference (13) as (C–H) wagging but the PED calculated in our research suggests that ν_{27} is mainly due to an asymmetric ring deformation and ν_{28} to a ring puckering.

(3) Finally, some modifications of Ansari and Singh's assignment are proposed for the region of the torsion vibrations, <

TABLE 9: Initial and Final Values of Scaling Factors According to SQM Method

coordinate number	unique scaling factor	refined unique scaling factor	initial scaling factor	refined scaling factor
1–6	0.92(8)	0.93(4)	0.92(2)	0.90(8)
7			0.92(2)	0.90(8)
8			0.92(2)	0.90(8)
9,13			1.04(2)	1.02(8)
10, 11, 12			0.92(0)	0.90(6)
14, 15, 16			0.92(0)	0.90(6)
17			0.99(0)	1.01(5)
18			0.99(0)	1.01(5)
19			0.99(0)	1.01(5)
20, 24			1.19(6)	1.19(4)
21, 22, 23			0.95(0)	0.94(8)
25			0.99(0)	0.98(8)
26, 27			0.95(0)	0.94(8)
28			0.99(0)	0.90(3)
29			0.91(5)	0.93(2)
30, 34			0.97(6)	0.97(0)
31, 32, 33			0.97(6)	0.97(0)
35			0.97(6)	0.97(0)
36			0.97(6)	0.97(0)
37			0.97(6)	0.97(0)
38			0.93(5)	0.98(2)
39			0.93(5)	0.93(0)
40			0.93(5)	0.93(0)
41			0.83(1)	0.78(4)
42			0.93(5)	0.88(9)

600 cm⁻¹. Thus, we described ν_{31} as a mixture of asymmetric ring torsion along with (C_{ring}–Cl) wagging but it is a ring deformation in reference (13). The modes ν_{32} , ν_{33} , ν_{37} , and ν_{39} are assigned for first time (to our knowledge) in this paper and described as appears in Table 7.

Conclusions

We have performed a theoretical analysis on the structure, torsional barrier and intramolecular interactions for 2,6-dichlorostyrene. The influence of the substituting halogens has been assessed in comparison to styrene and other monochlorostyrene derivatives. The nonplanarity of 2,6-dichlorostyrene has been explained on the basis of the balance among the attractive nuclear–electron, and repulsive nuclear–nuclear and electron–electron terms of the potential energy. Two twisted stable conformers are found with an energy barrier that strongly depends on the level of theory. MP2 overall torsion profile ($0 \leq \theta \leq 180^\circ$) enlarges the energy difference between planar and perpendicular ($\theta = 90^\circ$) rotamers while DFT results make them nearly energy-equivalent, regardless of the basis set, confirming this way the oversize of π -conjugation attained at this level of

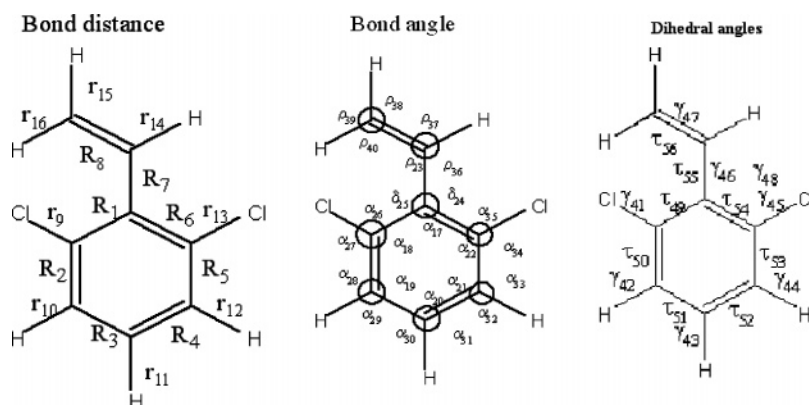
**Figure 11.** Natural Internal coordinates for 2,6-dichlorostyrene.

TABLE 10: Wavelength Linear Scaled, WLS, Frequencies and Relative Errors

mode	scaling factors	ν_{WLS}	ν_{obs}	relative error
1	0.91(8)	3000	3106	3.57
2	0.91(8)	2970	3099	3.91
3	0.91(9)	2966	3079	3.68
4	0.91(9)	2947	3055	3.56
5	0.92(0)	2930	3020	2.98
6	0.92(0)	2921	2992	2.36
7	0.95(8)	1642	1633	0.53
8	0.95(9)	1568	1582	0.86
9	0.96(0)	1542	1557	0.97
10	0.96(2)	1432	1445	0.90
11	0.96(3)	1422	1433	0.78
12	0.96(3)	1399	1402	0.25
13	0.96(6)	1314	1308	0.45
14	0.96(7)	1269	1258	0.84
15	0.96(8)	1208	1213	0.26
16	0.96(9)	1177	1187	0.83
17	0.97(0)	1148	1151	0.32
18	0.97(2)	1079	1091	1.14
19	0.97(2)	1066	1078	1.04
20	0.97(3)	1028	1034	0.55
21	0.97(4)	999	985	1.42
22	0.97(5)	949	966	1.72
23	0.97(6)	936	934	0.21
24	0.97(7)	884	895	1.28
25	0.98(0)	788	794	0.72
26	0.98(0)	774	781	0.92
27	0.98(0)	767	775	1.03
28	0.98(1)	742	741	0.17
29	0.98(4)	644	644	0.04
30	0.98(5)	597	600	0.60
31	0.98(6)	532	536	0.78
32	0.98(6)	528	532	0.73
33	0.98(8)	461	458	0.66
34	0.98(9)	415	417	0.46
35	0.99(0)	376	380	0.87
36	0.99(2)	334	338	1.18
37	0.99(3)	259	254	2.18
38	0.99(4)	221	219	1.14
39	0.99(5)	212	214	0.80
40	0.99(5)	201		
41	0.99(7)	107		
42	0.99(8)	69		

theory. On the basis of the partitioning of the total potential energy, the nature of the torsion barrier has been ascribed to the diminution of the attractive nuclear-electron energy and also to a decreasing of the so-called Coulomb term within the repulsive electron-electron energy. Natural bonding orbitals, NBO, allows to explain the energy barrier when the system is getting planar on the basis of the so-called Lewis term while when the system is markedly twisted the main factor seems to be the delocalization (or hyperconjugation) term. According to the charge-transfer chlorine lone-pair, $\text{LP}(\text{Cl}) \rightarrow \sigma^*(\text{C}-\text{C})_{\text{ring}}$ the twisted conformation is clearly more stable at MP2 level whereas for DFT the case is not so clear while vinyl-phenyl charge transfers are enhanced for the planar conformation. $\text{LP}(\text{Cl}) \rightarrow \sigma^*(\text{C}-\text{H})_{\text{vinyl}}$ charge-transfer plays a significant role at a planar conformation giving rise to weak $\text{Cl}\cdots(\text{H}-\text{C})_{\text{vinyl}}$ contacts that also predicts and topological analysis of electron density using AIM theory.

The Fourier decomposition of the torsional energy barrier concludes that the 4-fold V_4 and 2-fold V_2 terms mostly govern the shape of these energy plots. Accordingly, V_4 term is always barrier forming while V_2 , usually associated with hyperconjugative interactions, does so in the case of B3LYP/cc-pVTZ energy.

Also, in this work we have carried out for the first time a normal-mode analysis using SQM methodology for 2,6-dichlorostyrene. We have completed and corrected this way a previous analysis reported in the literature. Also, we have made a comparative analysis with the WLS and SQM methods, concluding that the results for the former are of the similar quality than those from the latter when using one unique scale factor. However the WLS method turns out to be a very useful tool for a fast first approach to the final analysis.

Acknowledgment. The authors thank the Spanish Ministerio de Educación y Ciencia (MEC) (Projects BQU2003-08221 and MAT2006-11267) and Consejería de Innovación, Ciencia y Empresa, Junta de Andalucía (PAI FQM337), for financial support. Also, the authors express their gratitude to Dr. Stewart Parker, ISIS Facility, for providing us the INS spectrum of the sample. Finally, we thank Mr. Francisco Hermoso for continuous technical help.

Supporting Information Available: Data concerning optimized and experimental geometries, relative energy values (kcal/mol), and absolute potential energy components (au) as a function of the vinyl-phenyl dihedral angle, important hyperconjugative interactions $\Delta E^{(2)}$ (kcal/mol), as well as diagonal force constants, both initial and refined, for 2,6-dichlorostyrene can be seen in Tables 1S–4S. This material is available free of charge via the Internet at <http://pubs.acs.org>.

References and Notes

- (1) Kennedy, J.; Zsuga, M. U.S. Patent 5,149,743.
- (2) Vanderbilt, D. P. PCT Int. Appl., 2000,77 pp.
- (3) Samyn, C. A.; Van den Broeck, K.; Gubbelmans, E.; Ballet, W.; Verbiest, T.; Persoons, A. *Opt. Mater.* **2003**, *21*, 67.
- (4) Michalek, J. C. Br. Patent 564828, 19441016, 1944.
- (5) Kasai, Y.; Sumi, H. Fr. Patent 2480948, 19811023, 1981.
- (6) Makhniashvili, I.; Koziel, E.; Fresenius, J. *Anal. Chem.* **2000**, *367*, 568.
- (7) Walsh, T. R.; Harkins, C. G.; Sutton, A. P. *J. Chem. Phys.* **2000**, *112*, 4402.
- (8) Scott, R. A.; Scheraga, H. A. *J. Chem. Phys.* **1965**, *42*, 2209.
- (9) Barfield, M.; MacDonald, C. J.; Peat, I. R.; Reynolds, W. F. *J. Am. Chem. Soc.* **1971**, *93*, 4195.
- (10) Rendell, J. C. T.; Burnell, E. E. *Mol. Phys.* **1997**, *90*, 541.
- (11) Rendell, J. C. T.; Zimmerman, D. S.; Van der Est, A. J.; Burnell, E. E. *Can. J. Chem.* **1997**, *75*, 1156.
- (12) Trovato, S.; Zuccarello, F.; Millefiori, S. *Boll. Acad. Gioenia Sci. Nat. Catania* **1973**, *11*, 173.
- (13) Ansari, B. J.; Singh, I. D. *Technology* **1971**, *8*, 253.
- (14) Nyquist, R. A. *Appl. Spectrosc.* **1986**, *40*, 196.
- (15) Granadino-Roldán, J. M.; Fernández-Gómez, M.; Navarro, A.; Jayasooriya, U. A. *Phys. Chem. Chem. Phys.* **2002**, *4*, 4890.
- (16) Granadino-Roldán, J. M.; Fernández-Gómez, M.; Navarro, A.; Jayasooriya, U. A. *Phys. Chem. Chem. Phys.* **2003**, *5*, 1760.
- (17) Granadino-Roldán, J. M.; Fernández-Gómez, M.; Navarro, A.; Peñarua, T.; Jayasooriya, U. A. *Phys. Chem. Chem. Phys.* **2004**, *6*, 1133.
- (18) Granadino-Roldán, J. M.; Fernández-Gómez, M.; Navarro, A.; Jayasooriya, U. A.; Mosteo, R. G.; Escribano, R. M. *J. Mol. Struct.* **2006**, *789*, 118.
- (19) Reed, A. E.; Curtiss, L. A.; Weinhold, F. *Chem. Rev.* **1988**, *88*, 899.
- (20) Bader, R. F. W. *Atoms in Molecules, A Quantum Theory*, Prentice Hall 2000.
- (21) Koch, U.; Popelier, P. L. A. *J. Phys. Chem.* **1995**, *99*, 9747.
- (22) Yoshida, H.; Ehara, A.; Matsuura, H. *Chem. Phys. Lett.* **2000**, *325*, 477.
- (23) Yoshida, H.; Takeda, K.; Okamura, J.; Ehara, A.; Matsuura, H. *J. Phys. Chem., A* **2002**, *106*, 3580.
- (24) Pulay, P.; Fogarasi, G.; Pongor, G.; Boggs, J. E.; Vargha, A. *J. Am. Chem. Soc.* **1983**, *105*, 2550.
- (25) Frisch, M. J., et al. *GAUSSIAN'03*, Revision C.01; Gaussian Inc.: Wallingford CT, 2004.
- (26) *GaussView3.07*; Gaussian Inc.: Pittsburgh, PA, 2000.

- (27) Hehre, W. J.; Radom, L.; Schleyer, P. v. R.; Pople, J. A. *Ab Initio Molecular Orbital Theory*; Wiley-Interscience: New York, 1986.
- (28) Kendall, R. A.; Dunning, T. H., Jr.; Harrison, R. J. *J. Chem. Phys.* **1992**, *96*, 6796.
- (29) Becke, A. D. *Chem. Phys.* **1993**, *98*, 5648.
- (30) Lee, C.; Yang, W.; Parr, R. G. *Phys. Rev., B* **1988**, *37*, 785.
- (31) Miehlich, B.; Savin, A.; Stoll, H.; Preuss, H. *Chem. Phys. Lett.* **1989**, *157*, 200.
- (32) Perdew, J.; Yang, Y. *Phys. Rev. B* **1992**, *45*, 13244.
- (33) Adamo, C.; Barone, V. *J. Chem. Phys.* **1998**, *108*, 664.
- (34) Glendening, E. D.; Reed, A. E.; Carpenter, J. E.; Weinhold, F. *NBO*, Version 3.1.
- (35) Biegler-König, F.; Schönbohm, J. *Comp. Chem.* **2002**, *23*, 1489. Biegler-König, F.; Schönbohm, J. *AIM2000*, Version 2.0 SBK Software 2002.
- (36) Hedberg, L.; Mills, I. M. *J. Mol. Spectrosc.* **1993**, *160*, 117.
- (37) Choi, C. H.; Kertesz, M. *J. Phys. Chem.* **1997**, *101A*, 3823.
- (38) Shen, Q.; Kuhns, J.; Hagen, K.; Richardson, A. D. *J. Mol. Struct.* **2001**, *567-568*, 73.
- (39) Sancho García, J. C.; Bredas, J. L.; Cornil, J. *Chem. Phys. Lett.* **2003**, *377*, 63.
- (40) Fabiano, E.; Della Sala, F. *Chem. Phys. Lett.* **2006**, *418*, 496.
- (41) Zhao, Y.; Truhlar, D. G. *J. Phys. Chem. A* **2006**, *110*, 10478.
- (42) Burke, K.; Perdew, J. P.; Wang, Y. In *Electronic Density Functional Theory: Recent Progress and New Directions*; Dobson, J. F., Vignale, G., Das, M. P., Eds.; Plenum: New York, 1998.
- (43) Sancho-García, J. C.; Pérez Jiménez, A. J. *J. Phys. B: At. Mol. Opt. Phys.* **2002**, *35*, 1509.
- (44) Sadlej-Sosnowska, N. *J. Phys. Chem. A* **2003**, *107*, 8671.
- (45) Pophristic, V.; Goodman, L. *J. Phys. Chem.* **2002**, *106*, 1642.
- (46) Cramers, C. J. *Essentials of Computational Chemistry. Theories and Models*; Wiley: Chichester, U.K., 2002.
- (47) Goodman, L.; Gu, H.; Pophristic, V. *J. Chem. Phys.* **1999**, *110*, 4268; Pophristic, V.; Goodman, L. *Nature* **2001**, *411*, 565.
- (48) Millefiori, S.; Alparone, A. *J. Chem. Soc., Faraday, Trans.* **1998**, *94*, 25.
- (49) Radom, L.; Pople, J. A. *J. Am. Chem. Soc.* **1970**, *92*, 4786.
- (50) Radom, L.; Hehre, W. J.; Pople, J. A. *J. Am. Chem. Soc.* **1972**, *94*, 2371.
- (51) Bond, D.; Schleyer, P. v. R. *J. Org. Chem.* **1990**, *55*, 1003.
- (52) Bader, R. F. W. *J. Phys. Chem. A* **1998**, *102*, 7314; *id. Chem. Eur. J.* **2006**, *12*, 2896.
- (53) Popelier, P. L. A. *J. Phys. Chem., A* **1998**, *102*, 1873.
- (54) Munshi, P.; Guru Row, T. N. *Cryst. Rev.* **2005**, *11*, 199.
- (55) Fogarasi, G.; Zhou, X.; Taylor, P. W.; Pulay, P. *J. Am. Chem. Soc.* **1992**, *114*, 8191.
- (56) Alcolea Palafox, M. *Recent Res. Devel. Phys. Chem.* **1998**, *2*, 213.
- (57) Panchenko, Y. N.; Stepanov, N. F. *Struct. Chem.* **2004**, *15*, 95.
- (58) Hilderbrand, R. L. *J. Mol. Spectrosc.* **1972**, *44*, 599.
- (59) Rauhut, G.; Pulay, P. *J. Phys. Chem.* **1995**, *99*, 3093.
- (60) Irikura, K. K.; Johnson, R. D., III; Kacker, R. N. *J. Phys. Chem. A* **2005**, *109*, 8430.